Reference:
Musa Alrefaya, Hichem Sahli, Iris Vanhamel, Dinh Nho Hao: A Nonlinear Probabilistic Curvature Motion Filter for Positron Emission Tomography Images. Scale Space and Variational Methods in Computer Vision-SSVM2009, LNCS 5567, PP. 212-223, 2009.

A Nonlinear Probabilistic Curvature Motion filter for Positron Emission Tomography Images

Musa Alrefaya[1], Hichem Sahli[1], Iris Vanhamel[1], and Dinh Nho Hao[1⋆]

Vrije Universiteit Brussel
Dept. Electronics and Informatics ETRO-IRIS
Pleinlaan 2
B-1050 Brussels, Belgium
malrefay, hsahli, iuvanham @ etro.vub.ac.be,
WWW home page: http://www.etro.vub.ac.be

Abstract. Positron Emission Tomography (PET) is an important nuclear medicine imaging technique which enhances the effectiveness of diagnosing many diseases. The raw-projection data, i.e. the sinogram, from which the PET is reconstructed, contains a very high level of Poisson noise. The latter complicates the PET image's interpretation which may lead to erroneous diagnoses. Suitable denoising techniques prior to reconstruction can significantly alleviate the problem. In this paper, we propose filtering the sinogram with a constraint curvature motion diffusion for which we compute the edge stopping function in terms of edge probability under the assumption of contamination by Poison noise. We demonstrate through simulations with images contaminated by Poisson noise that the performance of the proposed method substantially surpasses that of recently published methods, both visually and in terms of statistical measures.

1 Introduction

Positron Emission Tomography (PET) is an in vivo nuclear medicine imaging method that provides functional information of the body tissues. The PET image results from reconstructing very noisy, low resolution raw data, i.e. the sinogram, in which important features are shaped as a curved structures. Enhancing the PET image spurred a wide range of denoising models and algorithms. Some methodologies focus on enhancing the reconstructed PET image directly, where others prefer enhancing the sinogram prior to reconstruction. Existing methods may suffer drawbacks such as the careful selection of a high number of parameters, smoothing of the important features' boundaries, or prohibitive computation. Recently, nonlinear diffusion techniques have been investigated for PET images. Many researchers did explore the application of the well-known Perona

⋆ The authors sincerely wishes to express great thanks to Prof. M. Defrise, Division of Nuclear Medicine at AZ-VUB, for his discussions and feedback. The comparison to the TV-Nestrove scheme would not have been possible without the help of Dr. Pierre Weiss from INRIA-France, who did provide us the Matlab Code.

and Malik anisotropic diffusion [15] in combination with diverse diffusivity functions, on PET images [2, 4, 5, 14, 26], as well as on sinograms [6, 25]. The main drawback of this filter, with respect to the Poisson noise, which characterize such type of images, is that the diffusion produces important oscillations in the gradient, which finally leads to a poorly smoothed image [28, 29]. Moreover, the adopted diffusivity functions do not consider the special properties of the sinogram in which the preservation of the curved-shape features is paramount (see Figure1. In [28], mean curvature motion and Gaussian curvature motion of PET images have been investigated. Total variation (TV) scheme for smoothing the PET images was also discussed in [28]. Happonen et al. [29] propose filtering the sinogram in the *stackgram* domain where the signal along the sinusoidal trajectories of the sinogram can be filtered separately. They used and compared the Gaussian and nonlinear filters.

Filtering the sinogram has the advantage that the noise distribution is known, which is not the case after reconstruction. Consequently, this work proposes filtering the sinogram by means of a curvature constrained filter in which the amount of diffusion is modulated according to a probabilistic diffusivity function that suits images contaminated with Poisson noise. In addition, a comparison of the proposed method with TV-based methodologies proposed in [1] and [12], is conducted. For this purpose, a simulated thorax PET phantom was constructed to which varying levels of Poisson noise have been added is used. For evaluating the filtering approaches, contrast noise curves (contrast versus background noise at different iteration numbers) were generated for the different filtering approaches.

The reminder of the paper is organized as follows. Section 2, briefly review the notions of curvature motion, edge affected diffusion filtering, and self-snakes. The proposed filtering scheme is introduced in Sect. 3. Section 4.1 introduces the applied validation methods, the remainder of Sec.4 discusses the experimental results. Conclusions and future work are given in Sec.5.

2 Geometry Driven Scale-Space Filtering

This section reviews the formulations for mean curvature motion (MCM), Edge Affected Variable Conductance Diffusion (EA-VCD), and self-snakes. Let f be a scalar image defined on the spatial image domain Ω, then the family of diffused versions of f is given by:

$$U(f) : f(.) \rightarrow u(., t) \text{ with } u(., 0) = f(.) \tag{1}$$

where U is referred to as the scale-space filter, u is denoted the scale-space image, and the scale $t \in \mathbb{R}^+$ [23, 26]. The denoised or enhanced version of f, is a given $u(., t)$ that is closest to the unknown noise-free version of f.

2.1 Curvature Motion

One way of introducing smoothness in the curve is to let it evolve under its Euclidean curvature k. Mean curvature motion (MCM) is considered as the standard curvature evolution. MCM allows diffusion solely along the level-lines. In Gauge coordinates the corresponding PDE formulation is:

$$u_t(.,t) = u_{vv} = k|\nabla u| = \text{div}\left[\frac{\nabla u}{|\nabla u|}\right]|\nabla u| \tag{2}$$

Hence diffusion solely occurs along the v-axis.

2.2 Edge Affected Variable Conductance Diffusion

Variable Conductance filtering (VCD) is based on the diffusion with a variable conduction coefficient that controls the rate of diffusion [23]. In the case of Edge Affected-VCD (EA-VCD), the conductance coefficient is inversely proportional to the edgeness. Consequently it is commonly referred to as the edge stopping function (g), in which the edgeness is typically measured by the gradient magnitude. The EA-VCD is governed by:

$$u_t = \text{ div}\left[g(|\nabla u|)\nabla u\right] \tag{3}$$

The above PDE system together with the initial condition given in (1) is completed with homogenous von Neumann boundary condition on the boundary of the image domain. Note that the Perona and Malik's antitropic diffusion [15] is an EA-VCD.

2.3 Self-Snakes

Self-snakes are a variant of the MCM in which an edge-stopping function is introduced [19]. The main goal is preventing further shrinking of the level-lines once they have reached the important image edges. For scalar images, self-snakes are governed by:

$$u_t = |\nabla u|\text{div}\left[g(|\nabla u|)\frac{\nabla u}{|\nabla u|}\right] \tag{4}$$

This equation adopts the same boundary condition as (3). Furthermore, it can be decomposed in two parts [19, 23]:

$$\begin{array}{rl} u_t = g|\nabla u|\text{div}\left[\frac{\nabla u}{|\nabla u|}\right] & +(\nabla g).\nabla u \\ = gk|\nabla u| & +(\nabla g).\nabla u \end{array} \tag{5}$$

The first part describes a degenerate forward diffusion along the level lines, i.e. orthogonal to the local gradient; it allows preserving the edges. Additionally, the diffusion is limited in areas with high gradient magnitude and encouraged in smooth areas. Actually the first term is the constraint curvature motion. The second term can be viewed as a shock filter since it pushes the level-lines towards valleys of high gradient, acting as Osher's shock filter [18].

3 The Probabilistic Curvature Motion Filter

Based on (i) the curvature motion method, and (ii) a probabilistic diffusivity function, we presented in an earlier work [16], this section introduces the proposed filtering schemes for PET sinogram, considering the following characteristics:

1. The important features in the sinogram are curved structures with high contrast values. These represent the region of interests in the reconstructed PET image, e.g. tumor.
2. The weak edges in the sinogram are the edges that contains low contrast values. In other words, edges with small $|u_{ww}|$.
3. The noise in the sinogram is a priori identified as a Poisson noise.

The above presented schemes, namely, MCM (2), EA-VCD (3) and the Self-Snakes (5), can be derived using the following general equation:

$$u_t = g_1(|\nabla u|)u_{vv} + g_2(|\nabla u|)u_{ww} \tag{6}$$

where the second order Gauge derivatives of the image in the (vv) and (ww) directions are given by:

$$u_{vv} = \frac{u_{xx}u_y^2 - 2u_x u_y u_{xy} + u_{yy}u_x^2}{\left(u_x^2+u_y^2\right)} \qquad u_{ww} = \frac{u_{xx}u_y^2 + 2u_x u_y u_{xy} + u_{yy}u_x^2}{\left(u_x^2+u_y^2\right)} \tag{7}$$

Equation (6) comprises, a diffusion modulated by g_1 along the image edges (vv) (a smoothing term), and a diffusion adjustable by g_2 across the image edges (ww) (a sharpening term). Careful modeling of these terms allows efficiently denoising the PET sinograms, whilst keeping their interesting features. In the following sections, we propose the use of a probabilistic diffusivity function, and derive two diffusions schemes, for which we did apply the Gauge derivatives numerical approximation that was described in [23].

3.1 The Probabilistic Diffusivity Function

The main idea of the Probabilistic Diffusivity Function [16] is to express the diffusivity function as the probability that the observed gradient presents no edge of interest under a suitable marginal prior distribution for the noise-free gradient histogram. The diffusivity function was defined as:

$$g_{pr}(x) = A(1 - P(H_1|x)) \tag{8}$$

where the normalizing constant A is set to $A = 1/(1 - P(H_1|0))$ to ensure that $g_{pr}(0) = 1$; the hypothesis H_1 describes the notion whether an edge element of interest is present given the considered noise, and H_0 an edge element of interest is absent. Formally,

$$H_0 : y \leq \sigma_n, \text{ and } H_1 : y > \sigma_n \tag{9}$$

with y being the ideal, noise-free, gradient magnitude, and σ_n the noise standard deviation in the observed gradient image. In [16] it has been demonstrated that

$$g_{pr}(x) = (1 + \mu\eta(0))\frac{1}{1 + \mu\eta(x)} \tag{10}$$

where $\mu = P(H_1)/P(H_0)$ is the *prior odds*, and $\eta(x) = p(x|H1)/p(x|H0)$ is the likelihood ratio.

Considering a Laplacian prior $p(y) = \frac{\lambda}{2}e^{-\lambda|y|}$, we have $\mu = \left(e^{\lambda\sigma_n} - 1\right)^{-1}$ [16], and the parameter λ can be estimated as

$$\lambda = [0.5(\sigma^2 - \sigma_n^2)]^{-1/2} \tag{11}$$

with σ^2 denoting the variance of the noisy image, and σ_n^2, as defined above. Due to limited space, the reader is referred to [16] for the detailed expression of $\eta(x)$ in (10).

The proposed diffusivity function,(10), has no free parameters to optimize, and it fits well in the cluster of the reference backward-forward diffusivities. Indeed, for the considered PET sinograms, the noise standard deviation, σ_n,in 11 is being estimated as $\sigma_n^2 = Var(u_{Ln})$ where the image noise u_{Ln} is reconstructed from the two finest resolution levels coefficients by applying the wavelet decomposition of u, using daubechi(4) function.

3.2 Probabilistic Constraint Curvature Motion

For the probabilistic constraint curvature motion (PCCM), we start from a constraint version of mean curvature motion: the diffusion across the level lines is prohibited whilst the diffusion along the level-lines is controlled via the probabilistic diffusivity function (10):

$$u_t = g_{pr}(|\nabla u|)u_{vv} = g_{pr}(|\nabla u|)k|\nabla u| \tag{12}$$

Thus the function g_1 in (6) is chosen to be $g_1 \doteq g_{pr}$, for dealing with Poisson noise. This filter effectively smooths the image, as well as preserves edges of the important features such as lines, curve and flow-like structures.

By its nature, the PCCM cannot enhance the weak edges and/or features in the sinogram. The second term in (6) allows the sharpening. Consequently, we set $g_2 \doteq g_1'$. In this way, weak but important edges are enhanced whilst the noise is removed efficiently. Formally, the enhanced PCCM (ePCCM) is given by:

$$u_t = g_{pr}(|\nabla u|)u_{vv} + g_{pr}'(|\nabla u|)u_{ww} \tag{13}$$

3.3 Probabilistic Self Snakes (PSS)

It can be demonstrated that the diffusion of scalar images via EA-VCD can be decomposed into (5), moreover, it can be rewritten as [7, 23]:

$$u_t = g(|\nabla u|)u_{vv} + [g(|\nabla u|) + g'(|\nabla u|)|\nabla u|]\, u_{ww} \tag{14}$$

consolidating the properties of both the self-snakes and the EA-VCD into a single diffusion schema. Considering equation (6), and the proposed probabilistic diffusivity function, we have $g_1(x) \doteq g_{pr}(x)$, and the sharpening term, $g_2(x) \doteq g_{pr}(x) + xg'_{pr}(x)$.

This filter proves to be very effective and flexible for the sinogram image where the high contrast regions, which represent a tumor in the reconstructed PET, should be smoothed wisely without blurring the poor edges. Like EA-VCDT, the main advantage of this filter is that the average gray value of the image is not altered during the diffusion process which is a significant issue in the sinogram.

4 Experiments and Discussion

4.1 Introduction

The goal of the conducted experiments consists of measuring the performance of the proposed filtering methods, and studying their influence on the two commonly used PET reconstruction methods. The filtered back projection (FBP) [11], and the iterative ordered subset expectation maximization (OSEM) [8], respectively. The FBP algorithm is computationally efficient while the OSEM algorithm can incorporate easily prior information on the image to improve image quality. In our experiments, the reconstruction parameters of these algorithms are set as follows: the hamming parameter in the FBP method is 0.5, while for the OSEM, we use 16 subsets and run it for 4 iterations. In the following the reconstructed PET images are denoted by $\mathcal{U}_{\mathrm{F}}(t) = \mathrm{FBP}(u_t)$, and $\mathcal{U}_{\mathrm{O}}(t) = \mathrm{OSEM}(u_t)$, respectively, for a given enhanced sinogam u_t.

A simulated thorax PET phantom, containing three regions of interest (tumors) was constructed. To which varying levels of Poisson noise have been added and used for the evaluation. 50 realizations (noisy sinograms) with added noise level of $1\text{x}10^6$ coincident events, have been generated. Each sinogram has a size of 256x256 pixels and their spacing is $2\text{x}2\frac{\text{mm}}{\text{pixel}}$. Figure.1(a) shows the ideal noise-free sinogram with the PET images obtain via the FBP (Fig.1(c)) and, OSEM (Fig.1(d)) reconstruction. A corresponding noise contaminated realization is shown in Fig.1(b),(e)-(f).

The proposed PCCM and PSS diffusion schemes have been assessed and evaluated against resent Total Variation (TV) denoising techniques, namely, the approach of Chambolle [1], denoted here after as **TV-C**, and the Nesterov [12] algorithm, denoted as **TV-N**.

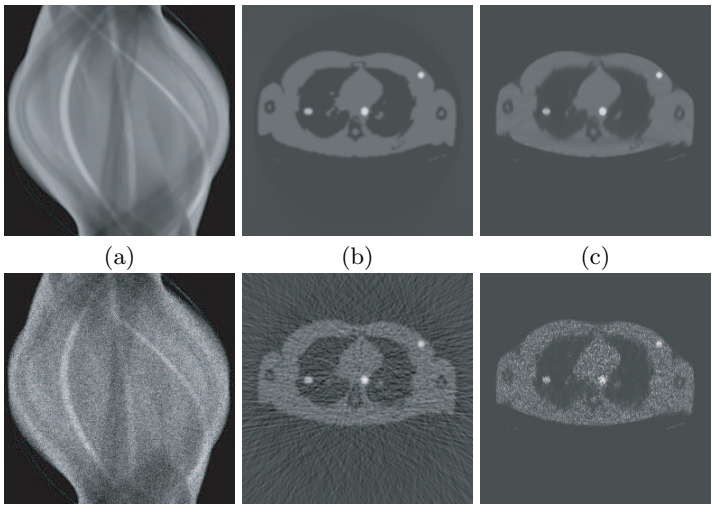

Fig. 1. (a) Original simulated sinogram and its reconstructed PET image using (b) FBP (c) OSEM reconstruction. (d) An example of one realization of a noisy sinogram and (e-f) the corresponding reconstructed PET images. The tumors (ROI) are the 3 clearly visible white spots.

4.2 Quantitative Evaluation Measures

Two types of evaluation measures are adopted. The first set stems from measuring the quality of the filtering techniques whilst the second set originates from validating the quality of the PET reconstruction. As ground-truth information, the former uses the noise-free image, whilst the latter needs prior identification of the important areas by a medical professional.

Denoising Quality The idea is to verify the quality of the denoised sinogram, u_t, with respect to the noise-free image I. In this work, we adopt the following measures [22]:

DQ1 The Peak Signal to Noise Ratio (**PSNR**) is a statistical measure of error, used to determine the quality of the filtered images. It represents the ratio of a signal power to the noise power corrupting. Obviously, one sees that the higher the PSNR, the better the quality.

$$PSNR(t) = 10\log_{10}\frac{\text{Card}(\Omega)}{\sum\limits_{p\in\Omega}|I(p)-u_t(p)|} \tag{15}$$

DQ2 The correlation ($\mathcal{C}_{\mathbf{m}\rho}$) between the noise-free and the filtered image. The higher this correlation the better the quality is.

$$\mathcal{C}_{m\rho}(t) = \rho\left[I, u_t\right] \tag{16}$$

DQ3 The calculated variance of the noise (**NV**) describes the remaining noise-level. Therefore, it should be as small as possible.

$$\mathrm{NV}(t) = Var\left(|I - u_t|\right) \tag{17}$$

In this work, we are interested in comparing the maximum of each measure for the different filtering approaches. The latter yields the best obtainable result per measure.

The Contrast Recovery Curve For evaluating the filtering on the reconstructed PET images, the filtered data, at discrete scales for the proposed PDE approaches, and regularization parameters values, for the TV approaches, were reconstructed using the FBP and the OSEM approaches. With the reconstructed data sets we determine the *contrast recovery curve* using a set of region of interests that were identified by a medical professional. In our case, the 3 white spots that represent tumors in Fig.1. This was accomplished by quantifying a Contrast Gain, cg, and coefficients of variations Var_{cg}. We calculate the contrast gain cg_i for each realizations $i \in [1, N = 50]$ and its overall variance. Let $R = \{r_1, r_2, \ldots, r_n\}$ be the set of identified ROIs ($n = 3$ in our case), and B a representative background tissue area,then:

$$\begin{aligned} cg_i(t) &= \tfrac{1}{n} \sum_{r \in R} \tfrac{1}{\mathrm{Card}(r)} \sum_{p \in r} \mathcal{U}^{(i)}(p,t) - \tfrac{1}{\mathrm{Card}(B)} \sum_{p \in B} \mathcal{U}^{(i)}(p,t) \\ Var_{cg}(t) &= \tfrac{1}{N} \sum_{i=1}^{N} (cg_i(t) - \tfrac{1}{N} \sum_{j=1}^{N} cg_j(t))^2 \end{aligned} \tag{18}$$

where p is a pixel. The Var_{cg} versus cg plot provides a straightforward evaluation method for the contrast-noise tradeoff [3]. The best quality PET reconstruction is situated in the upper, i.e. high contrast gain, left, i.e. high stability, area of the plot.

4.3 Evaluation

A fundamental issue with scale-spaces induced by diffusion processes, as the ones proposed in this paper, is the automatic selection of the most salient scale. For our PET sinogram denoising application, we use an earlier proposed optimal scale selection approach [22], where the maximum correlation method has been adopted:

$$t_{opt} = \mathrm{argmax}\left[\widehat{\mathcal{C}}_{mp}(t)\right] = \mathrm{argmax}\left[\sigma[u_t] + \frac{\sigma[n_o(t_0)]}{\sigma[u_{t_0}]}\sigma[n_o(t)]\right] \tag{19}$$

withn_o is the so-called outlier noise, which we estimated using the proposed wavelet-based noise estimation. Note that, t_0 is the zeroth scale, thus $u_{t_0} = f$ and $n(t_0)$ represents the initial amount of noise.

Figures 2.(a),(d) illustrates the obtained optimal scale using the PSS approach, and and the TV-C results, respectively. The Table 1 lists the quantitative results comparing the different denoising approaches. The best performing filtering method, per measure is, displayed in bold. As it can be seen, the best performing filtering is achieved when using the PSS. Furthermore, we notice that for all the used measures, the proposed diffusion methods outperform the considered TV-based filters.

Table 1. Denoising quality measures v.s. filtering approaches.

	f	PCCM	ePCCM	PSS	TV-C	TV-N
$PSNR(t_{opt})$	-17.510	-4.1000	-4.1000	**-3.9900**	-5.7200	-5.1100
NV(t_{opt})	7.5100	1.6000	1.6000	**1.5500**	1.9300	1.8000
$\mathcal{C}_{m\rho}(t_{opt})$	0.8500	0.9915	0.9916	**0.9917**	0.9876	0.9890

Figure 3 depicts the Contrast Recovery Curves for the investigated filtering methods. Recall that, the best enhancement is obtained when the contrast gain is as high as possible whilst the variance over it remains as small as possible. Furthermore, the degree of smoothness of the curve indicates the stability and biasing level.

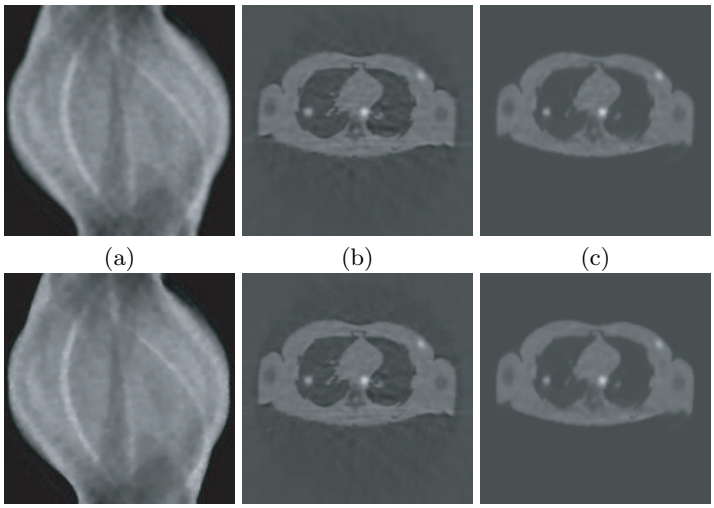

Fig. 2. Enhanced sinogram and reconstructed PET images. PSS-based approach first row, TV-based approach second row.

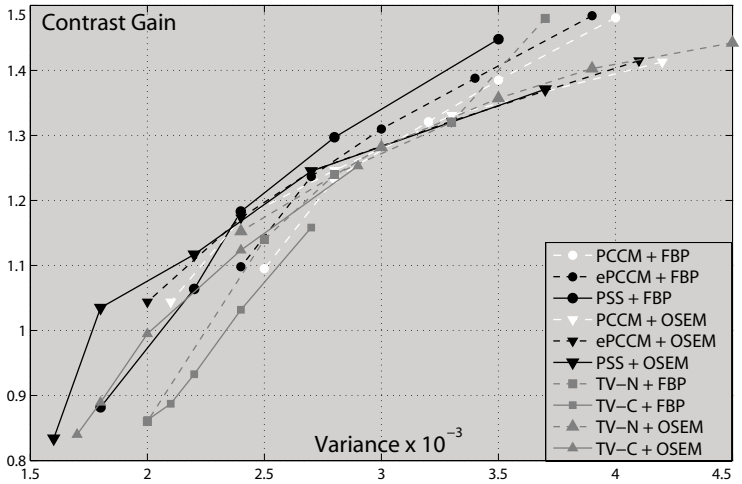

Fig. 3. The contrast-noise curve. The best performance occurs in the area where the contrast gain is high and its variance is low.

We may observe that all investigated methods have a good performance. However, the proposed PSS yields the best performance on the given data set.

5 Conclusions

Experiments results show that combining the probabilistic diffusivity function with the curvature motion diffusion produces a powerful nonlinear filtering method that is appropriate for PET sinograms. It preserves the boundaries of the curvy shape features and wisely smoothes the regions of interest as well as the other regions. Our findings show that the PCCM method smoothes the PET images and keeps the boundaries of the important features, while the weak edges in some cases are vanished. On the other hand, the ePCCM method overcome this problem and the contrast recovered better in the ROIs by the enhancing term in the filter. This filter gives a well smoothed image and preserves the edges, and gains the advantage of the curvature motion diffusion and the shock filter. The PSS approach deal better with the problem of the poor and discontinuity of edges which is common in the PET images. Using the probabilistic diffusion function has proven to be an effective and suitable tool for controlling the diffusion process in the proposed scheme. The results, as shown in the contrast-noise curves, demonstrate that this function has a great capability to detect and enhance the important features edge's in the high noisy sinogram images. Moreover, The proposed diffusivity function has no free parameters to optimize. All parameters are image-based, and are automatically estimated and proved to give the the best results.

References

1. Chambolle, A.: An Algorithm for Total Variation Minimization and Applications. JMIV, 20:89-97, (2004)
2. Chan, T., Li, H., Lysaker M., and Tai X. C.: Level Set Method for Positron Emission Tomography. International Journal of Biomedical Imaging Volume 2007, (2007)
3. Comtat, C., Kinahan, P. E., Fessler, J. , Beyer, T., Townsend, D., W., M., Defrise, , and Michel, C.: Clinically feasible reconstruction of 3D whole-body PET/CT data using blurred anatomical labels. Phys Med Biol 47, pp. 1-20, (2002)
4. Demirkaya O.: Diffusion Filtering of Functional Images using the structural information available in Hyprid imaging modalities , IEEE Medical Imaging Symposium- Germany, (2008)
5. Demirkaya, O.: Post-reconstruction filtering of positron emission tomography whole-body emission images and attenuation maps using nonlinear diffusion filtering. Acad Radiol. 11:1105-1114, (2004)
6. Demirkaya, O.: Anisotropic diffusion filtering of PET attenuation data to improve emission images. Physics in Medicine Biology 47(20):271-8, (2002)
7. Didas, S., Weickert, J.,: Combining Curvature Motion and Edge-Preserving Denoising. First International Conference on Scale Space Methods and Variational Methods in Computer Vision, 568-579, (2007)
8. Hudson, M., Larkin, R.: Accelerated image reconstruction using ordered subsets of projection data. IEEE Trans. Med. Imag., vol. 13, no. 4, pp. 601 609, (1994).
9. Happonen, A. P., Koskinen, M. O.: Experimental Investigation of Angular Stackgram Filtering for Noise Reduction of SPECT Projection Data: Study with Linear and Nonlinear Filters. International Journal of Biomedical Imaging, Vol. 2007, (2007)
10. Jonsson E., Huang, S. C., Chan T.: Total Variation Regularization in Positron Emission Tomography. UCLA, Tech. Rep. no. 48, (1998).
11. Kak, C. A., Slaney, M.: Principles of Computerized Tomographic Imaging.IEEE Press, (1999)
12. Nesterov, Y.: Smooth minimization of non-smooth functions. Mathematic Programming, Series A, 103:127-152, (2005)
13. Osher, S., Sethian, J. A.: Fronts propagating with curvature-dependent speed: algorithms based on Hamilton Jacobi formulations. Journal of Computational Physics, vol. 79, no. 1, pp. 12-49, (1988)
14. Padfield, D. R., Manjeshwar, R.: Adaptive conductance filtering for spatially varying noise in PET images. Progress in biomedical optics and imaging, vol. 7(3),nO. 30, (2006)
15. Perona, P. and Malik, J.: Scale space and edge detection using anisotropic diffusion, IEEE Transactions on Pattern Analysis and Machine Intelligence, vol. 12, pp. 629-639, (1990)
16. Pizurica, A., , Vanhamel, I., Sahli, H., Philips, W., Katartzis, A.: A Bayesian formulation of edge-stopping functions in non-linear diffusion, IEEE Signal Processing Letters, vol. 13 (8), pp. 501-504, (2006)
17. Rudin, L.I., Osher, S., Fatemi., E.: Nonlinear total variation based noise removal algorithms. Physica D, 60:259268, (1992)
18. Rudin, L.I. and Osher, S.: Feature-oriented image enhancement with shock filters. Technical Report, Department of Computer Science, California Institute of Technology, (1989).

19. Sapiro, G.: Geometric partial differential equations and image analysis. University Press, Cambridge, (2001)
20. Sumengen, B., Manjunath, B. S.: Edgeflow-driven Variational Image Segmentation: Theory and Performance Evaluation. Technical Reperot, Department of Electrical and Computer Engineering University of California, Santa Barbara, (2006)
21. Turkheimer F. E., Boussion N., Anderson A. N., Pavese N., Piccini P., Visvikis, D.: PET Image Denoising Using a Synergistic Multiresolution Analysis of Structural (MRI/CT) and Functional Datasets, The Journal of nuclear medicine,49:657-666,(2008)
22. Vanhamel, I., Mihai, C., Sahli, H., Katartzis A., Pratikakis, I.: Scale Selection for Compact Scale-Space Representation of Vector-Valued Images. Vol. 4485, International Journal of Computer Vision, (2008)
23. Vanhamel, I.: Vector valued nonlinear diffusion and its application to image segmentation Ph.D. Thesis, Vrije Universiteit Brussel, Faculty of Engineering Sciences, Electronics and Informatics (ETRO), (2006)
24. Wang, Y., and Zhou, H.: Total Variation Wavelet-Based Medical Image Denoising. International Journal of Biomedical Imaging, Vol. 2006 (2006)
25. Wang, W.: Anisotropic Diffusion Filtering for Reconstruction of Poisson Noisy Sinograms. Volume 2(11):16-23 Journal of Communication and Computer, (2005)
26. Weickert J.:, Anisotropic diffusion in image processing, ECMI Series. Teubner-Verlag, Stuttgart, Germany, (1998)
27. Weiss, P., Aubert, G., Blanc-Fraud, L.: Efficient schemes for total variation minimization under constraints in image processing. Technical Report 6260, INRIA (2007)
28. Zhu, H., Shu, H., Zhou, J., Bao, X., Luo, L.: Bayesian algorithms for PET image reconstruction with mean curvature and Gauss curvature diffusion regularizations. Computers in Biology and Medicine , Volume 37 , Issue 6 , Pages 793 - 804, (2007)
29. Zhu, H., Shu H., Zhou, J., Toumoulin, C., Luo, L.: Image reconstruction for positron emission tomography using fuzzy nonlinear anisotropic diffusion penalty. Med Biol Eng Comput., 44(11): 983-997, (2006)